

EXPERIMENTAL STUDY ON STRUCTURAL, MICROSTRUCTURAL AND ELECTRICAL CONDUCTIVITY OF MAGNESIUM DOPED NICKEL-COPPER-ZINC FERRITES

Kyaw Kyaw¹, Aye Aye Lwin², Moe Min Min Aye³ and Win Kyaw⁴

Abstract

Magnesium doped Nickel-Copper-Zinc ferrites with the general formula $\text{Ni}_{0.6-x}\text{Mg}_x\text{Cu}_{0.2}\text{Zn}_{0.2}\text{Fe}_2\text{O}_4$ (where $x = 0.0 - 0.6$ with the step of 0.2) were prepared by solid state reaction method. The samples were characterized by X-ray Diffractometry (XRD), Scanning Electron Microscopy (SEM) and temperature dependent electrical conductivity measurement. XRD confirmed the presence of spinel phase cubic crystalline as major phase of the as-prepared samples. The lattice parameters and average crystallite sizes of the samples were investigated from the observed XRD patterns. The samples were made into pellets and the temperature dependent dc electrical conductivities were studied by using two-probe method. Electrical conduction mechanism and the activation energy were studied. The obtained electrical conductivity results reveal that the samples ($x = 0.0, 0.2$ and 0.4) were normal ionic conductors and the sample $x = 0.6$ was superionic conductor at high temperature.

Keywords: $\text{Ni}_{0.6-x}\text{Mg}_x\text{Cu}_{0.2}\text{Zn}_{0.2}\text{Fe}_2\text{O}_4$, solid state reaction, XRD, SEM, conduction mechanism, superionic conductor.

Introduction

Spinel of the type $\text{M}^{2+}\text{M}_2^{3+}\text{O}_4$ attract the research interest because of their versatile practical applications [Iftimie, (2006)]. In the case of $\text{M}^{3+} = \text{Fe}$, the resulting spinel ferrites having a general chemical composition of MFe_2O_4 ($\text{M} = \text{Mg}, \text{Ni}, \text{Cu}, \text{Zn}, \text{Mn}, \text{Co}, \text{Cd}, \text{etc.}$) are widely used as magnetic materials [Kony, (2004)].

The polycrystalline NiMgCuZn soft ferrites are suitable for core materials in microinductor applications. In view of the extensive applications of NiCuZn ferrite [Rajendra, (2014)], it is economical to replace Nickel with Magnesium and achieve desirable properties in NiMgCuZn ferrites. MgCuZn ferrite is a pertinent magnetic material suitable for high-frequency applications owing to its properties like high resistivity, fairly high Curie transition temperature, environmental stability, and low cost [Ramana, (2012)]. In the present work, Magnesium doped Nickel-Copper-Zinc ferrites, $\text{Ni}_{0.6-x}\text{Mg}_x\text{Cu}_{0.2}\text{Zn}_{0.2}\text{Fe}_2\text{O}_4$ (where $x = 0.0, 0.2, 0.4$ and 0.6) were prepared by solid state reaction method and their structural, microstructural and electrical properties were investigated in the temperature range of 303 K – 773 K.

Materials and Method

Preparation of Samples

Magnesium doped Nickel-Copper-Zinc ferrites, $\text{Ni}_{0.6-x}\text{Mg}_x\text{Cu}_{0.2}\text{Zn}_{0.2}\text{Fe}_2\text{O}_4$ (where $x = 0.0, 0.2, 0.4$ and 0.6) were prepared by solid state reaction method. Starting materials of Analytical Reagent (AR) grade Magnesium Oxide (MgO), Nickel Oxide (NiO), Copper Oxide

¹ Dr, Assistant Lecturer, Department of Physics, Taungoo University

² Dr, Associate Professor, Department of Physics, Loikaw University

³ Dr, Associate Professor, Department of Physics, Technological University (Dawei)

⁴ Dr, Associate Professor, Department of Physics, Pyay University

(CuO), Zinc Oxide (ZnO) and Ferric Oxide (Fe_2O_3) were used to prepare the samples. Then, the starting materials were weighed with desired stoichiometric compositions and mixed each other. The mixed starting materials were heated at 1000°C for 5 h in JLabTech Electric Oven. Figure 1 shows the flow diagram of the sample preparation process.

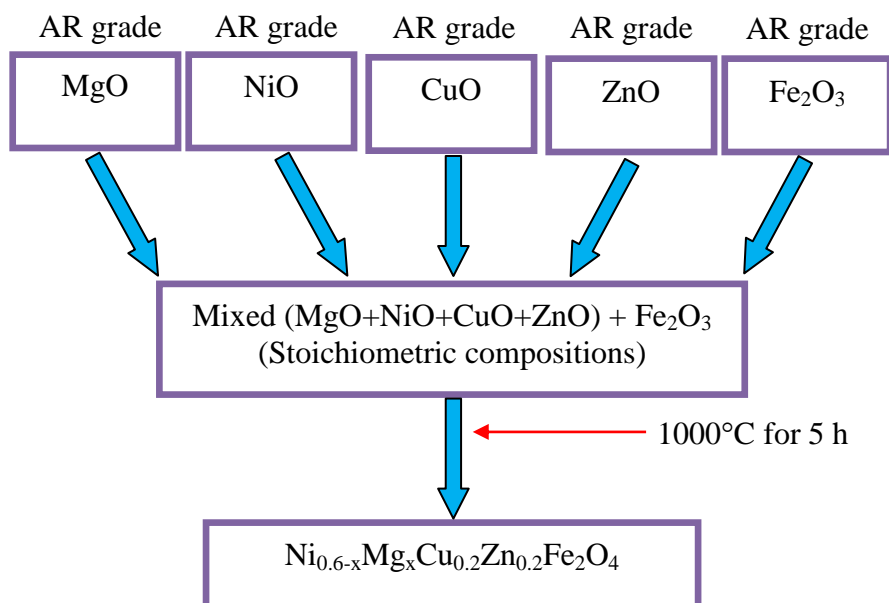


Figure 1 Flow-diagram of the $\text{Ni}_{0.6-x}\text{Mg}_x\text{Cu}_{0.2}\text{Zn}_{0.2}\text{Fe}_2\text{O}_4$ sample preparation process

XRD and SEM Measurements

The crystalline phase formation, variation of the lattice parameters and estimation of the crystallite sizes of the Magnesium doped Nickel-Copper-Zinc ferrites, $\text{Ni}_{0.6-x}\text{Mg}_x\text{Cu}_{0.2}\text{Zn}_{0.2}\text{Fe}_2\text{O}_4$ (where $x = 0.0, 0.2, 0.4$ and 0.6) were investigated by PC-controlled RIGAKU MULTIFLEX X-ray Diffractometer [Universities' Research Centre (URC), University of Yangon] using Ni-filter with $\text{CuK}\alpha$ radiation, $\lambda = 1.54056 \text{ \AA}$. Microstructural properties of the samples were investigated by using JEOL JSM-5610LV SEM [Universities' Research Centre (URC), University of Yangon] with the accelerating voltage of 15 kV, the beam current of 50 mA and 5500 times of photo magnification.

Temperature Dependent Electrical Resistance Measurement

Firstly, the as-prepared samples were made into pellets by SPECAC hydraulic pellet-maker using 5 ton ($\sim 70 \text{ MPa}$). The electrical resistances of the samples were observed by using FLUKE 180 digital multi-meter in the temperature range of 303 K – 773 K by the use of DELTA A SERIES DTA-4896 Temperature Controller. The area and thickness of the pellets were $1.14 \times 10^{-4} \text{ m}^2$ and 5.15 mm respectively. Experimental setup of the electrical conductivity measurement is shown in Figure 2.

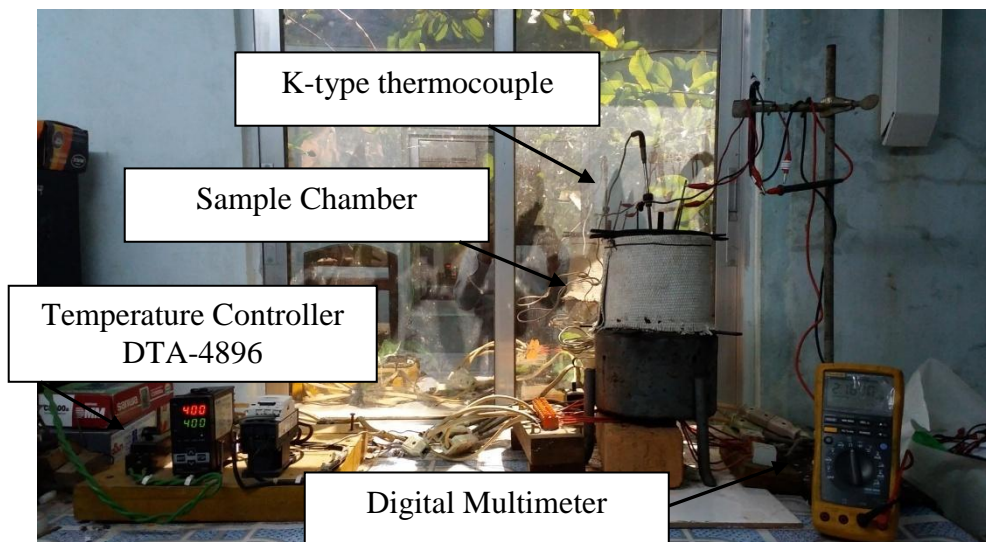


Figure 2 Experimental setup of temperature dependent electrical resistance measurement

Results and Discussion

Structural Investigation

The indexed powder X-ray diffraction patterns of the samples are shown in Figure 3. For phase identification of the samples, the collected diffraction lines were identified by using reference patterns of pure substances or JCPDS data files of (i) Cat. No. 22-1012>Franklinite - syn, $ZnFe_2O_4$, Cat. No. 88-1943>Magnesioferrite - syn, $MgFe_2O_4$, Cat. No. 25-0283>Cuprospinel, $CuFe_2O_4$ and Cat. No. 10-0325>Trevorite - syn, $NiFe_2O_4$ for $x = 0.0, 0.2, 0.4$ samples and (ii) Cat. No. 22-1012>Franklinite - syn, $ZnFe_2O_4$, Cat. No. 25-0283>Cuprospinel, $CuFe_2O_4$ and Cat. No. 10-0325>Trevorite - syn, $NiFe_2O_4$ for $x = 0.6$ sample.

XRD patterns show the formation of single phase cubic structure with dominant peak corresponding to (311) reflection indicating that the crystallites are preferentially oriented along (311) plane. The lattice parameters are evaluated by using crystal utility of the equation

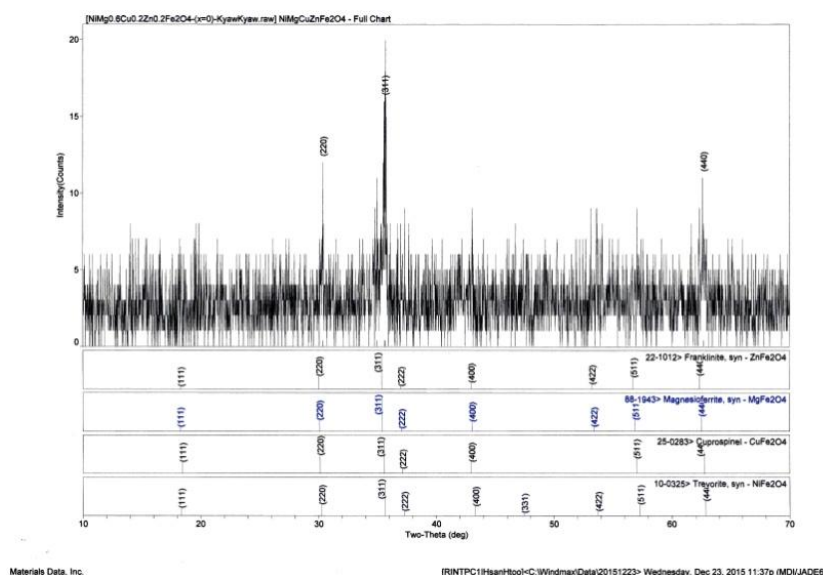


Figure 3 (a) XRD pattern of $Ni_{0.6-x}Mg_xCu_{0.2}Zn_{0.2}Fe_2O_4$ where $x = 0.0$

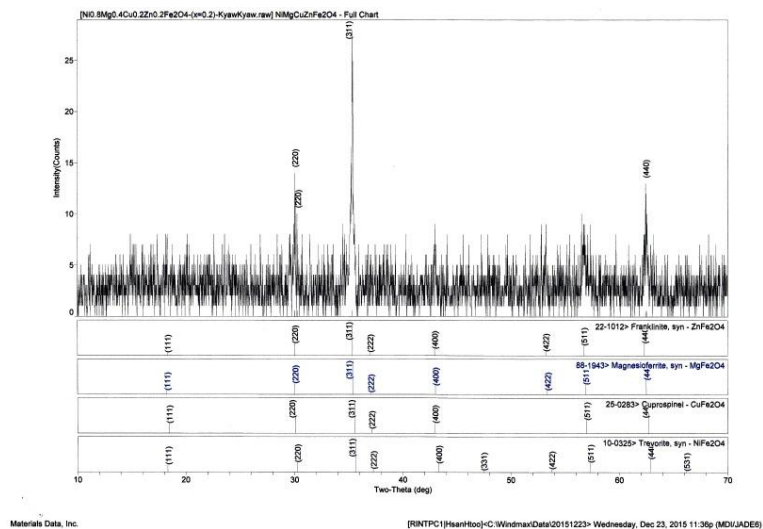


Figure 3(b) XRD pattern of $\text{Ni}_{0.6-x}\text{Mg}_x\text{Cu}_{0.2}\text{Zn}_{0.2}\text{Fe}_2\text{O}_4$ where $x = 0.2$

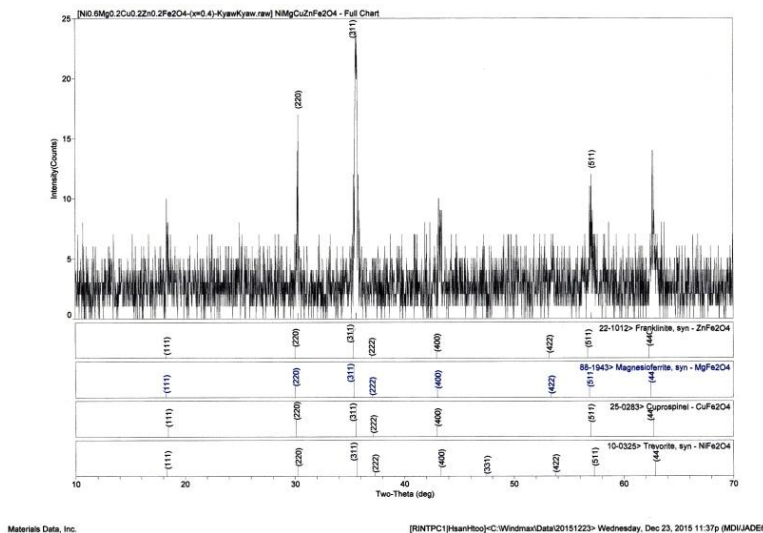


Figure 3(c) XRD pattern of $\text{Ni}_{0.6-x}\text{Mg}_x\text{Cu}_{0.2}\text{Zn}_{0.2}\text{Fe}_2\text{O}_4$ where $x = 0.4$

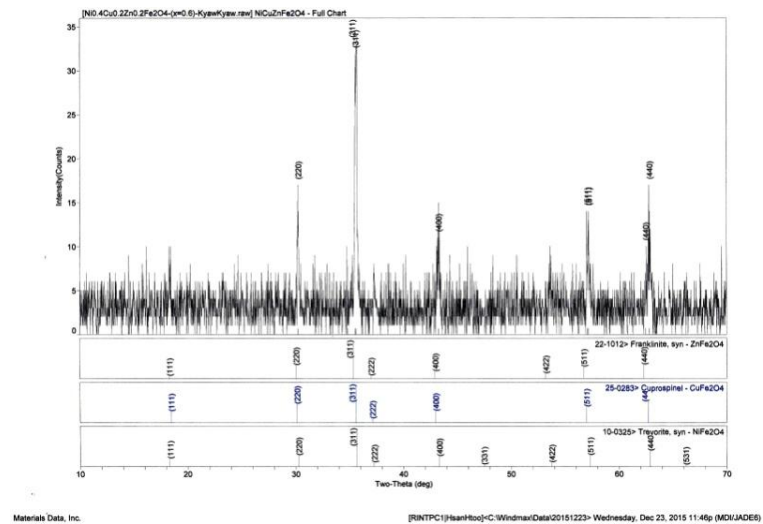


Figure 3(d) XRD pattern of $\text{Ni}_{0.6-x}\text{Mg}_x\text{Cu}_{0.2}\text{Zn}_{0.2}\text{Fe}_2\text{O}_4$ where $x = 0.6$

Table 1 The lattice parameters and crystallite sizes of $\text{Ni}_{0.6-x}\text{Mg}_x\text{Cu}_{0.2}\text{Zn}_{0.2}\text{Fe}_2\text{O}_4$

Sample (Contents x of Mg)	Obs. $a=b=c$ (Å)	D (nm)
0.0	8.3518	46.54
0.2	8.3907	64.94
0.4	8.3599	45.69
0.6	8.3608	53.04

of $\frac{\sin^2 \theta}{(h^2 + k^2 + l^2)} = \frac{\lambda^2}{4a^2}$ where θ is the diffraction angle ($^\circ$), (hkl) is the miller indices, λ is the wavelength of incident X-ray (Å) and a is the lattice parameter of the samples (Å). The observed lattice parameters are tabulated in Table 1. Figure 4 shows the variation of the lattice parameters with Mg concentration of the samples. The lattice parameters of the samples were found to be alternated with increase in concentration of Mg due to the ionic substitution of Mg^{2+} on Ni^{2+} in the lattice sites. It can be simply explained as follows:

The atomic sites distribution of $\text{Ni}_{0.6-x}\text{Mg}_x\text{Cu}_{0.2}\text{Zn}_{0.2}\text{Fe}_2\text{O}_4$ ferrites can be taken as $(\text{Ni}_{0.6-x}\text{Cu}_{0.2}\text{Zn}_{0.2}\text{Fe})[\text{Mg}_x\text{Cu}_{0.2}\text{Zn}_{0.2}\text{Fe}]\text{O}_4$ where the brackets () and [] denote A-site and B-site respectively. Such cation distribution is based on the following facts:

- (1) Ni^{2+} ions have a strong preference to occupy the A-site while Mg^{2+} ions have a strong preference to occupy the B-site.
- (2) As for Mg-ion distribution, it is reported that Ni^{2+} ions strongly prefer to occupy the A-site for low Mg-concentration. However, for high Mg-concentration, it is suggested that the Ni^{2+} ions are either distributed between A-site and B-site or reside at the grain boundaries. Thus, according to the assumed cation distribution, increasing of the Mg-concentration from $x = 0.1$ to $x = 0.3$ leads Fe^{3+} content in A-site to decrease and that in B-site to increase.

Ramana, M.V. et al (2012) has reported that the lattice parameters of the $\text{Ni}_{0.6-x}\text{Mg}_x\text{Cu}_{0.1}\text{Zn}_{0.3}\text{Fe}_2\text{O}_4$ (for $x = 0.0, 0.1$ and 0.2) ferrites are 8.36 Å, 8.38 Å and 8.35 Å respectively. Thus, in this work, the obtained lattice parameters are acceptable due to the agreement with the results of Ramana, M.V. et al (2012).

The crystallite sizes of the samples were estimated by using the Scherrer formula, $D = \frac{0.9\lambda}{B \cos \theta}$ where D is the crystallite size (nm), λ is the wavelength of incident X-ray (Å), θ is the diffraction angle of the peak under consideration at FWHM ($^\circ$) and B is the observed FWHM (radians). The breadth of the Bragg peak is a combination of both instrument and sample dependent effects. To decouple these contributions, it is necessary to collect a diffraction pattern from the line broadening of a standard material such as silicon to determine the instrumental broadening. In this work, the instrumental effects on the breadth of the Bragg peak neglected. In the present work, the average crystallite sizes of the samples are also presented in Table 1. The obtained crystallite sizes are 46.54 nm for $x = 0.0$, 64.94 nm for $x = 0.2$, 45.69 nm for $x = 0.4$ and 53.04 nm for $x = 0.6$ respectively. It indicates the nanosized Cu-Mg ferrites materials. The variation of the crystallite sizes with Mg concentration of $\text{Ni}_{0.6-x}\text{Mg}_x\text{Cu}_{0.2}\text{Zn}_{0.2}\text{Fe}_2\text{O}_4$ (for $x = 0.0, 0.2, 0.4$ and 0.6) ferrites is shown in Figure 4.

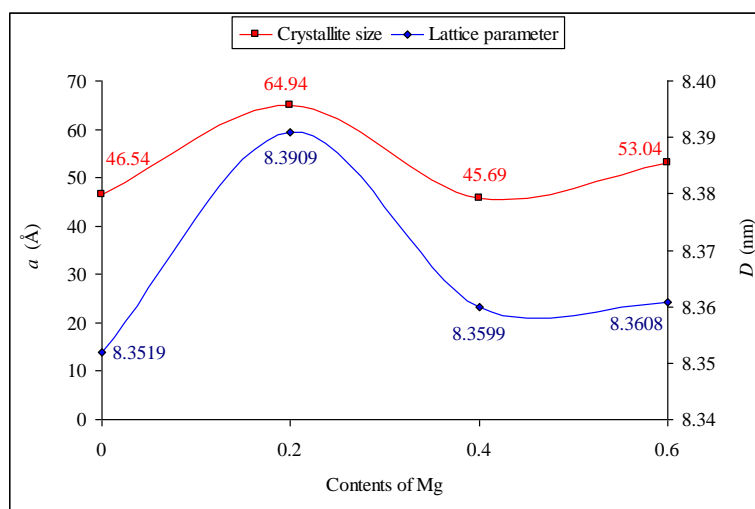


Figure 4 Variation of the lattice parameters and crystallite sizes with Mg concentration of $\text{Ni}_{0.6-x}\text{Mg}_x\text{Cu}_{0.2}\text{Zn}_{0.2}\text{Fe}_2\text{O}_4$

SEM Analysis

Scanning Electron Microscopy (SEM) was employed for microstructural characteristics of $\text{Ni}_{0.6-x}\text{Mg}_x\text{Cu}_{0.2}\text{Zn}_{0.2}\text{Fe}_2\text{O}_4$ (for $x = 0.0, 0.2, 0.4$ and 0.6) powders. Figure 5 shows the SEM micrographs of the samples.

As shown in observed SEM micrographs, generally, morphological features of the samples are spherical shape of different grain sizes. The grain sizes varied with the concentration of Mg^{2+} on NiCuZn ferrite.

In Figure 5(a), the grain sizes of the samples are in the range of $0.40 \mu\text{m} - 1.80 \mu\text{m}$. Most of the grains are found to be non-homogeneous and some of the grains are composed of agglomerated particles. The area of the pores (porosity) is about 10% of the image.

As shown in Figure 5(b), the grain sizes of the samples are obtained as in the range of $0.20 \mu\text{m} - 0.50 \mu\text{m}$. Some of the grains are agglomerated particles with poor grain boundary. The pore area is about 15% of the image.

In Figure 5(c), the grain sizes are in the range of $0.20 \mu\text{m} - 0.40 \mu\text{m}$ and thus the sample is the most homogeneous in the investigated samples. The pore area is about 5% of the image and it is the smallest area of pores with poor grain boundary of the sample.

In Figure 5(d), the grain sizes are $0.25 \mu\text{m} - 0.50 \mu\text{m}$ range. Most of the defects or the largest area of pores is found in the sample and it is about 40% area of the image. In this image, the grain boundary is also poor. The grain sizes of the samples are listed in Table 2.

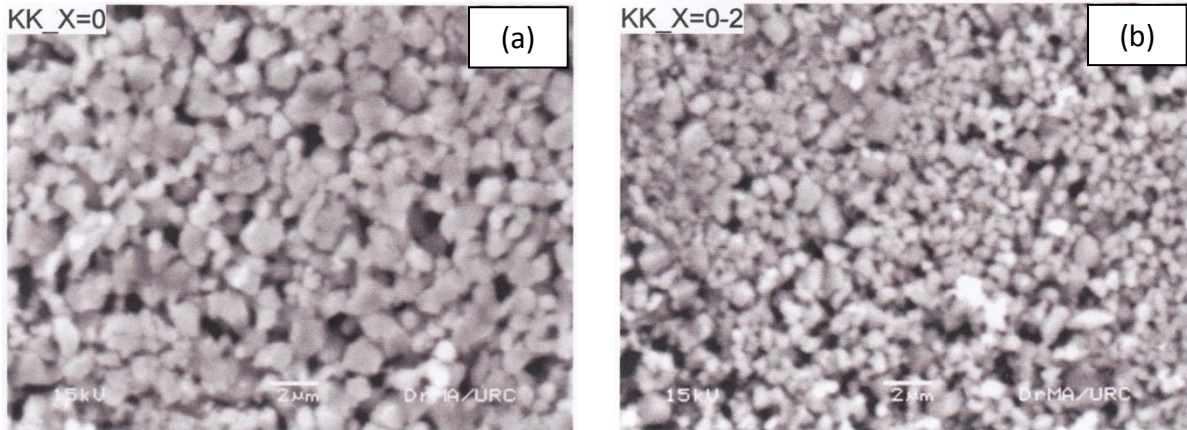


Figure 5. SEM micrographs of Ni_{0.6-x}Mg_xCu_{0.2}Zn_{0.2}Fe₂O₄ where (a) x = 0.0 and (b) x = 0.2

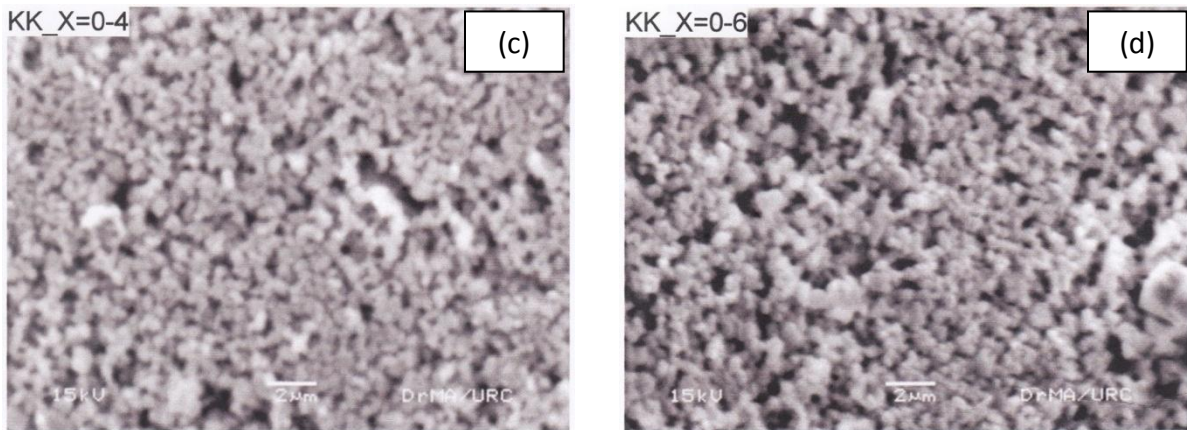


Figure 5 SEM micrographs of Ni_{0.6-x}Mg_xCu_{0.2}Zn_{0.2}Fe₂O₄ where (c) x = 0.4 and (d) x = 0.6

Table 2 Grain sizes of the Ni_{0.6-x}Mg_xCu_{0.2}Zn_{0.2}Fe₂O₄

Sample (Contents x of Mg)	Grain sizes (μm)
0.0	0.40 – 1.80
0.2	0.20 – 0.50
0.4	0.20 – 0.40
0.6	0.25 – 0.50

Temperature Dependence Electrical Conductivity Study

The superionic conductivity of the materials plays an important role in the class of solid electrolytes. Most of the spinel based compounds are well-known superionic conductors. The samples are cubic structures at room temperature. Since, the substances have been found to be characterized by a higher conductivity ($10^{-5} - 10^{-4} \text{ S cm}^{-1}$) in the high temperatures due to the ionic motion caused by ionic-bond disorder (so called fast ionic conductors or superionic conductors).

Electrical conductivity of a ceramic with temperature obeys an Arrhenius expression $\sigma = \sigma_0 \exp(-E_a/kT)$, where σ is the conductivity, σ_0 is the pre-exponential factor, E_a is the activation energy for ionic conduction, k is the Boltzmann constant and T is the absolute

temperature. In the present work, Arrhenius plots of the variation of dc electrical conductivity of the $\text{Ni}_{0.6-x}\text{Mg}_x\text{Cu}_{0.2}\text{Zn}_{0.2}\text{Fe}_2\text{O}_4$ (for $x = 0.0, 0.2, 0.4$ and 0.6) samples are shown in Figure 6.

According to the theory of ionic conductivity, the slopes of the electrical conductivity in each of the $\ln \sigma$ vs. $1000/T$ graph, e.g., in Figure 6(a) (for $x=0.0$ or $\text{Ni}_{0.6}\text{Cu}_{0.2}\text{Zn}_{0.2}\text{Fe}_2\text{O}_4$),

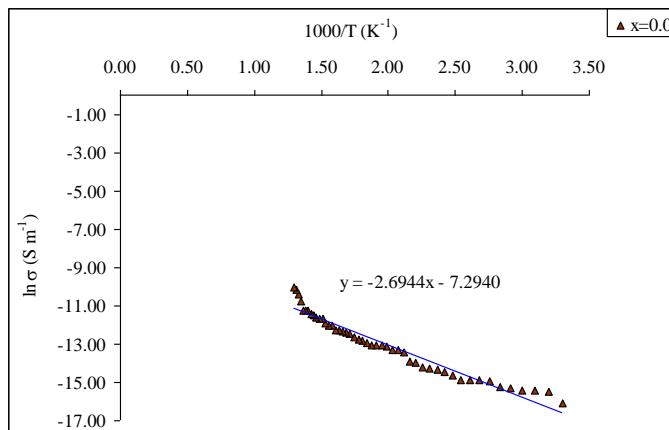


Figure 6 (a) Arrhenius plot of the $\ln \sigma$ versus $1000/T$ graph of the $\text{Ni}_{0.6-x}\text{Mg}_x\text{Cu}_{0.2}\text{Zn}_{0.2}\text{Fe}_2\text{O}_4$ where $x = 0.0$

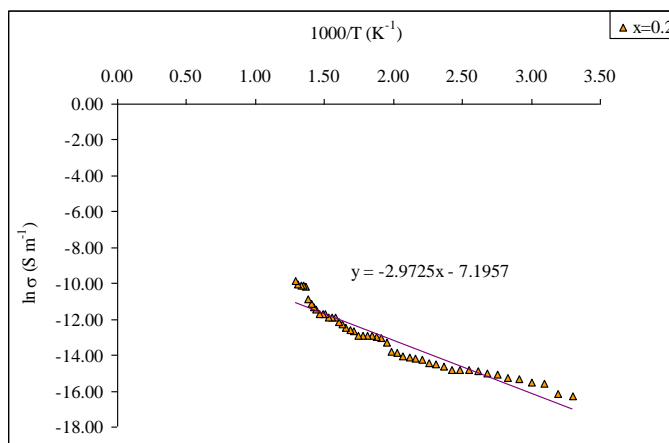


Figure 6(b) Arrhenius plot of the $\ln \sigma$ versus $1000/T$ graph of the $\text{Ni}_{0.6-x}\text{Mg}_x\text{Cu}_{0.2}\text{Zn}_{0.2}\text{Fe}_2\text{O}_4$ where $x = 0.2$

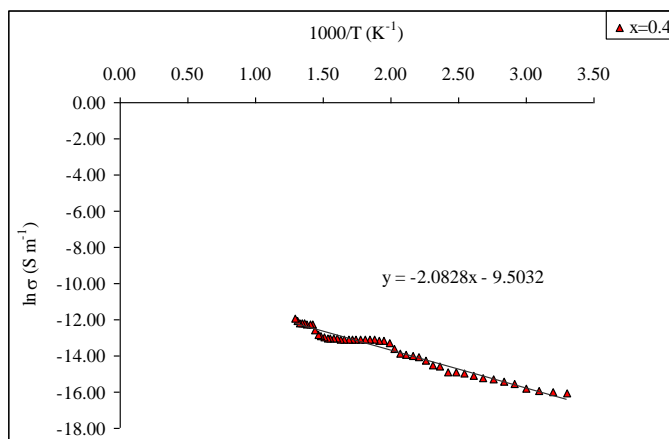


Figure 6 (c) Arrhenius plot of the $\ln \sigma$ versus $1000/T$ graph of the $\text{Ni}_{0.6-x}\text{Mg}_x\text{Cu}_{0.2}\text{Zn}_{0.2}\text{Fe}_2\text{O}_4$ where $x = 0.4$

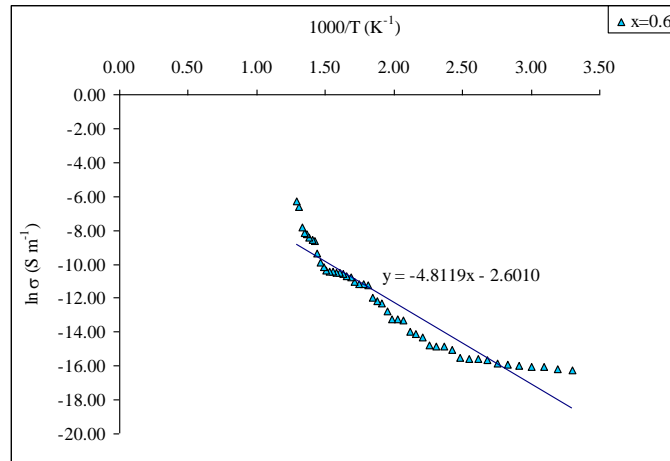


Figure 6 (d) Arrhenius plot of the $\ln \sigma$ versus $1000/T$ graph of the $\text{Ni}_{0.6-x}\text{Mg}_x\text{Cu}_{0.2}\text{Zn}_{0.2}\text{Fe}_2\text{O}_4$ where $x = 0.6$

corresponding to the activation energy for creating of defect states due to the ionic motions of the sample. The electrical conductivity (σ) of the sample can be written in the form:

$$\begin{aligned} \sigma &= \sigma_0 \exp(-E_a / kT) \\ \ln(\sigma) &= -E_a / kT + \ln \sigma_0 \\ &= (-E_a / k)(1/T) + \ln \sigma_0 \end{aligned}$$

From Figure 6(a), the activation energy E_a can be obtained by using the slope of the $\ln \sigma$ versus $1000/T$ graph.

$$\begin{aligned} E_a/k &= 2.6944 \times 1000 \\ E_a &= 2.6944 \times 1000 \times k \\ E_a &= 2.6944 \times 1000 \times 1.38 \times 10^{-23} \\ E_a &= 3.7183 \times 10^{-20} \text{ J} \\ E_a &= 0.2324 \text{ eV} \end{aligned}$$

As shown in figures, the electrical conductivity of the samples increased with increase in temperature. The activation energies of the samples are listed in Table 3.

In general, for the ferrite samples, the activation energy is often associated with the variation of mobility of charge carriers rather than with their concentration. The charge carriers are considered as residing at the vacant sites and conduction occurs via a hopping process which depends upon the activation energy. Due to addition of Mg^{2+} inter ionic distance increase which enhances the barrier height encountered by the charge carriers during the hopping process and consequently, it enhances the activation energy.

Table 3 Slopes of $\ln \sigma$ vs. $1000/T$ graphs and the activation energies of the $\text{Ni}_{0.6-x}\text{Mg}_x\text{Cu}_{0.2}\text{Zn}_{0.2}\text{Fe}_2\text{O}_4$

Sample (Contents x of Mg)	Slope of $\ln \sigma$ vs. $1000/T$ graph	Activation energy (eV)
0.0	2.6944	0.2324
0.2	2.9725	0.2564
0.4	2.0828	0.1796
0.6	4.8119	0.4150

According to literature of electrical conductivity, the electrical conductivity of a solid is $\sigma \geq 10^{-3} \text{ S m}^{-1}$, the sample is known as the solid electrolyte material or superionic conductor or fast ion conductor. From the observed experimental data of electrical conductivity measurements, the ($x = 0.0, 0.2$ and 0.4) samples are normal ionic conductors and the sample $x = 0.6$ is a superionic conductor at high temperature due to its electrical conductivity is $1.33 \times 10^{-3} \text{ S m}^{-1}$ at 763 K . The $\ln \sigma$ vs $1000/T$ curves of the samples indicate the charge carrier density which are generated as a consequence of thermal activated process of lattice defects, is increased up to end point temperature by increasing the concentration of the Mg^{2+} .

Conclusion

Magnesium doped Nickel-Copper-Zinc ferrites, $\text{Ni}_{0.6-x}\text{Mg}_x\text{Cu}_{0.2}\text{Zn}_{0.2}\text{Fe}_2\text{O}_4$ (where $x = 0.0, 0.2, 0.4$ and 0.6) were successfully prepared by solid state reaction method. The as-prepared samples were characterized by XRD and SEM to study the effect of dopant concentration of Mg^{2+} structural and microstructural characteristics of Ni-Cu-Zn ferrites. The X-ray diffraction confirmed the presence of spinel type cubic crystalline as major phase of the as-prepared samples. The lattice parameters were found to be alternated with the increase in concentration of Mg. The crystallite sizes were estimated by using the Scherrer formula and nanosized ferrite crystallites of the samples were obtained and these were also alternated. From the SEM micrographs, the grain shapes of the samples are found to be spherical with non-uniform grain sizes. Most of the pores are appeared with different sizes of area. The grain sizes of the samples varied with the dopant concentration of Mg^{2+} . The grain size of the undoped material was found to be the largest one among the investigated samples. From the temperature dependence electrical conductivities results, the samples $x = 0.0, 0.2$ and 0.4 were normal ionic conductors and $x = 0.6$ sample was superionic conductor at the high temperature. Thus, the $x = 0.6$ sample can be used as the solid electrolyte material.

Acknowledgements

The authors would like to acknowledge Professor Dr Khin Khin Win, Head of Department of Physics, University of Yangon, for her valuable suggestion and comments for this work. I would like to thank Professor Dr Nge Nge Khaing, Head of Department of Physics, Taungoo University, for her kind permission to carry out this work.

References

- Ifimie, N., Rezlescu, E., Popa, P.D. & Rezlescu, E. (2006) Gas sensitivity nanocrystalline nickel ferrite. JOURNAL OF OPTOELECTRONICS AND ADVANCED MATERIALS, 8(3), 1016-1018.
- Kony, D.E. (2004). Dielectric Relaxation in Al - Substituted Ni - Cd Spinel Ferrites. Egypt Journal of Solids, 27, 285-296.
- Rajendra, R., Pushpinder, B. & Rajlakshmi, N. (2014). Structural and Electrical Properties of Titanium Substituted Ni-Cu-Zn Ferrites. International Journal of Chemical and Physical Sciences, 3, 132-138.
- Ramana, M.V., Reddy, N.R. & Kumar, K.V.S. (2012). Influence of Magnesium Substitution on Thermal and Electrical Properties of NiCuZn Ferrites for Microinductor Core Applications. Physics Research International, 10, 1-8.